THE JOURNAL OF PHYSICAL CHEMISTRY B

Article

pubs.acs.org/JPCB

Angular Dependence of Surfactant-Mediated Forces Between Carbon Nanotubes

Dirk Müter,*[,†] Panagiotis Angelikopoulos,[†,‡] and Henry Bock[†]

[†]Department of Chemical Engineering, Heriot-Watt University, Edinburgh, United Kingdom

[‡]Computational Science & Engineering Laboratory, Swiss Federal Institute of Technology, Zürich, Switzerland

ABSTRACT: We employ dissipative particle dynamics to examine surfactant-mediated forces between two carbon nanotubes. Calculations are performed varying both the distance and the angle between the nanotubes. For small distances, a repulsive region is observed, followed by an overall attractive interval with strong oscillations in the force. Decreasing the angle between the tubes leads to a steady increase in the force, but the relative dependence on the separation distance is preserved. We find that the force scales linearly with the size of the overlap area between the tubes. This allows us to express the angle dependence by a simple equation, whereas the distance dependence is represented by a master curve. For the parallel case, the behavior is significantly different.

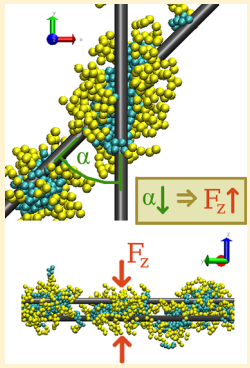

INTRODUCTION

Since their discovery more than 20 years ago, carbon nanotubes (CNTs) have excelled at setting new records for electrical and mechanical material properties, for example, a Young's modulus of >1 TPa[1] for single-wall carbon nanotubes (SWCNTs). These outstanding properties have fueled the interest of scientists for applications, ranging from the biomedical sector[2,3] to drug delivery systems,[4] sensors,[5,6] and composites,[7,8] yet most of the record-setting values were measured on individual CNTs. Although nowadays CNTs up to many millimeters in length can be produced,[9] a material consisting mostly of carbon nanotubes would rely on a network of carbon nanotubes in which the macroscopic properties would be dominated by the behavior of the joints between the individual tubes.

When dispersed in aqueous solution, CNTs form bundles of tubes due to the strong tube/tube van der Waals (vdW) forces. Using ultrasonication individual tubes can be produced from those bundles[10] when a stabilizing agent is present to prevent rebundling. As a stabilizer, amphiphilic molecules, such as copolymers and surfactants,[11,12] can be used. Because of the strong hydrophobicity, the surfactants adsorb on the tube surfaces with their hydrophobic tails, whereas head groups point outward, thus rendering the coated tubes hydrophilic. This leads to a repulsion between the surfactant covered tubes, which effectively shields them from each other. This effect has been studied intensively over various experimental accessible parameters such as concentration, surfactant geometry, and surfactant chemistry. Apart from experimental studies,[13−15] surfactant-decorated CNTs have also been examined in computer simulations both atomistically[16−18] and coarse-grained on the mesoscale.[19,20]

Mesoscale simulations by Angelikopoulos et al. confirmed the experimental findings that surfactant-decorated CNTs repel each other.[21] They also showed that at surfactant concentrations below the critical micellar concentration (CMC) surfactants will predominantly adsorb onto the junction formed by a pair of crossing tubes.[22] Interestingly, their simulations found that the force exerted by the surfactant aggregate *can* be repulsive for larger tube/tube separation but is *always* attractive for smaller separation distances.[23,24] This behavior indicates that surfactants can also be used to stabilize a 2D or 3D network of CNTs by effectively gluing the tubes together at their crossing points. However, all of their simulations investigated only the perpendicular arrangement of the tubes. Knowledge and understanding of how the angle between the tubes affects adsorption, aggregation, and the forces between the tubes is still lacking.

In this article, we are going to resolve this issue by employing the same simulation setup as in ref 25, that is, a dissipative particle dynamics (DPD) simulation with a coarse-grain model of the surfactant. Varying the angle from perpendicular to parallel and the distance between the CNTs, we examine the forces between the tubes and analyze how the surfactant aggregation is affected.

MODEL AND SIMULATION

The model and simulation setup have been discussed in detail elsewhere,[22,25] and thus here we can focus on the key points. Surfactant molecules are represented by chains of beads consisting of five hydrophilic head beads (H5) and five hydrophobic tail beads (T5), leading to an amphiphilic molecule H5T5. To simulate the bonds between neighboring

Received: September 12, 2012
Revised: October 31, 2012

   dx.doi.org/10.1021/jp309074c | *J. Phys. Chem. B* XXXX, XXX, XXX−XXX

Table 1. Parameters and Settings Used in This Work[a]

surfactants	tail beads = 5	head beads = 5	σ = 1.0
	σ_{bond} = 1.2 σ	ε_{bond} = 4.0 ε	ε = 1.0
nanotubes	r_{CNT} = 1.0 σ	ε_{CNT} = 2.5 ε	d = 3.0−15.0 σ
simulation	temp. = 0.7 ε/k_B	Δt = 0.01	r_{cut} (L-J) = 2.5 σ
	DPD-ξ = 1.0	DPD-r_{cut} = 2.5 σ	r_{cut} (WCA) = $2^{1/6}$ σ
	$N_{molecules}$ = 300, 500	Box-z = 200 σ	Box-x × Box-y = 10 000 σ^2
	equilibr. = 3 × 10^7 Δt	prod. = 2 × 10^7 Δt	

[a]See the text for further explanations.

beads in the chain, a spring potential is employed $\Phi_{Bond}(r) = \varepsilon_{Bond}(r-r_{Bond})^2$, with r_{Bond} representing the bond length and ε_{Bond} representing the depth of the potential. All beads in the system interact with each other using an empiric potential, which in the case of interactions between the hydrophobic beads, is given by the well-known Lennard-Jones (LJ) (12,6) potential, where ε is the depth of the potential and σ is the particle diameter:

$$\phi_{LJ}(r) = 4\varepsilon\left[\left(\frac{\sigma}{r}\right)^{12} - \left(\frac{\sigma}{r}\right)^{6}\right]$$

For all other interactions (tail/head and head/head), the LJ potential is truncated at its minimum at the distance $r_{cut} = 2^{1/6}\sigma$ (WCA = Weeks−Chanders−Andersen potential). Therefore, the derivative of the potential, the force, is zero here, and the force is repulsive only. These interactions represent the solvent implicitly.

The carbon nanotubes are in this coarse-grained model treated as smooth cylinders and interact with the beads over the LJ potential for hydrophobic beads and the WCA potential for the hydrophilic beads. In both cases, the potential is shifted to the surface of the tube and acts along the line of shortest distance between the beads and the tube axis, that is, normal to the tube surface. The interaction strength with the tubes can be adjusted by a multiplicative factor ε_{CNT}. Table 1 summarizes the parameters used in our simulation.

The tubes are placed in the lower part of the simulation box at a variable separation distance, d, whereas the upper part is considered to be "bulk". The CNTs are fixed in their positions during the simulation. A snapshot of the simulation setup is depicted in Figure 1. Because we are interested in the angular

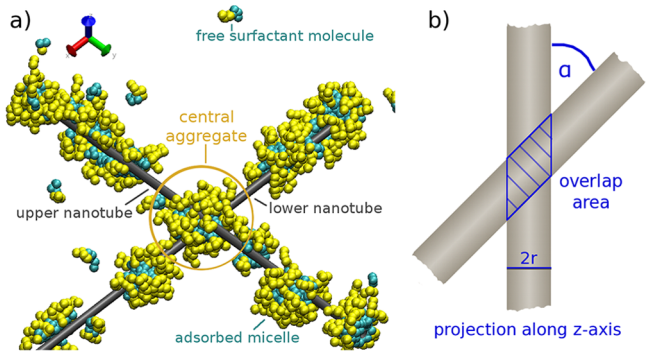

Figure 1. Left: Schematic of the simulation setup showing two perpendicularly arranged carbon nanotubes with adsorbed surfactant micelles and free surfactant molecules; the hydrophilic head groups are colored in yellow, while the hydrophobic tails are given in cyan. Right: Sketch of two angled tubes in the projection along the z axis visualizing the definitions of the angle and overlap area.

dependence of the force, the angle α in the x−y plane between the nanotubes is adjusted to the following values: 90, 67.5, 45, 22.5, 9, and 0°. For angles other than the parallel, diagonal (45°), or perpendicular case, the size of the simulation box has to be adjusted to ensure uninterrupted and smooth continuation of the tubes into the next periodic image of the box. The box size is then chosen in such a way that the box volume is constant for all simulations. Furthermore, for these cases, the nonzero thickness of the tubes has to be taken into account by introducing two small tube pieces on the corners of the box opposite to the angled tube.

The simulation itself is performed in the canonical ensemble (constant number of particles, volume, and temperature) using the DPD approach.[26] In DPD, the temperature is controlled by introducing a dissipative and a random force between all interacting beads. A detailed description of the DPD forces for our system is given in ref 25. All simulations are performed at bulk concentrations well below the CMC (CMC = 5.2 × 10^{-5} σ^{-3})[25] with a fixed number of particles (300 ≈ 0.3 × CMC and 500 ≈ 0.5 × CMC). Naturally, the bulk concentration will fluctuate slightly when using a constant number of particles. Our simulations show that these deviations are within reasonable limits of ±10% of the mean value. Keeping the number of molecules constant avoids any issues with inserting and deleting molecules.

To quantify the aggregation of the surfactants on the tubes, we calculate cluster size distributions:

$$P(N) = \left\langle \frac{n_N}{\sum_{N=0}^{\infty} n_N} \right\rangle$$

with n_N as the instantaneous number of clusters of size N, and $P(N)$ is the probability of finding a cluster of size N.

We also require a definition for "adsorbed": a surfactant molecule is considered to be adsorbed when itself or one molecule in the same cluster has a tail bead that is <1.5 σ away from the nanotube surface. Likewise, two molecules are counted as belonging to the same cluster if the distance between one tail bead of the first molecule and at least one tail bead of the other molecule is <1.5 σ.

Special attention is paid to the central aggregate, which is defined as the cluster that is adsorbed on both nanotubes simultaneously. More than one central aggregate may exist particularly in the parallel case. On parallel tubes, the central aggregate can also be infinite for high surfactant coverages because of the periodic boundary conditions rendering the tubes effectively infinite.

Here we study the surfactant-mediated force between two tubes given as the canonical ensemble average of the sum of the z-component of all individual bead/tube forces

dx.doi.org/10.1021/jp309074c | J. Phys. Chem. B XXXX, XXX, XXX−XXX

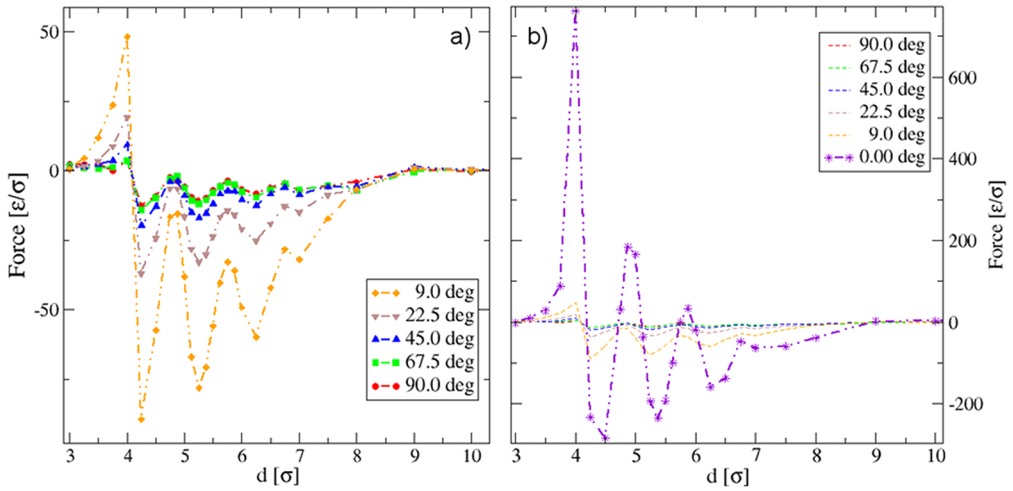

Figure 2. (a) z-component of the force acting on the upper nanotube as a function of the tube/tube separation d for different angles as indicated in the Figure. The force curves are dominated by strong oscillations and an attractive region between 4 $\sigma < d < 9\ \sigma$ for all angles >0. (b) Zoomed out version of panel a showing also the parallel case (tube length = 100 σ). In the parallel case, the force oscillates in the region 4 $\sigma < d < 9\ \sigma$ around a constant value, which allows the force to reach repulsive values.

$$F_z = \langle \sum_{i=1}^{N} \sum_{k=1}^{N_{beads}} f_z(i, k) \rangle$$

where the first sum runs over all molecules i and the second sum runs over all beads k in i. Here we report the force on the upper nanotube. Thus, a negative force indicates an effective attraction between the tubes, whereas positive values correspond to repulsion. The forces on the lower tube were found to be equal in magnitude within 15% of the force on the upper tube and of opposite sign, as they must according to Newton's third law.

RESULTS AND DISCUSSION

Surfactants adsorb and aggregate at the outer surface of the carbon nanotubes (Figure 1) and thereby modify the interaction between the tubes.[20,22] This is relevant for the dispersion of carbon nanotubes as well as the development of novel materials. Until now, only two pairwise conformations: parallel[16,17] and perpendicular[19,22−24] have been considered. Here we study the dependence of the tube/tube cohesive force on the angle between the tubes.

In Figure 2, the dependence of the z-component of the surfactant mediated tube/tube force on the distance between the tubes axes is shown for six angles ranging from 0 (parallel tubes) to 90° (perpendicular tubes). It is immediately obvious that the force curves for all angled cases (9−90°) are very similar (Figure 2a), whereas the parallel case included in Figure 2b appears to be somewhat different.

All curves show an initial repulsive region for distances of up to 4σ followed by an overall attractive region between approximately 4 σ and 9 σ. Superposed onto this general behavior are strong oscillations. This behavior has been analyzed in detail for the perpendicular case in ref 25. In brief, the overall attraction is essentially a restoring force produced by the central aggregate as a response to stretching deformation due to increasing the distance between the tubes. The oscillations are due to layering, that is, well-known packing effects in confined systems such as slit-pores.[27] At distances larger than ~9 σ the surfactant-mediated force vanishes as there are large gaps between the adsorbed aggregates at the low concentrations studied here.

The parallel case is distinctly different from all angled cases. In the parallel case, the "central aggregate" extends over the entire tube, whereas it is relatively small and finite for angled tubes, as seen in the snapshots in Figure 7. This results in some important deviations of the behavior of the parallel case (Figure 2b). First, the magnitude of the force becomes a function of the tube length because the aggregate that is able to mediate the force, the one that is adsorbed on both tubes, can extend over the whole tube. Putting finite size effects aside, the magnitude of the force is thus simply linear dependent on the tube length for any given concentration. Second and most importantly, the overall attractive region is almost completely absent. This is rather interesting and might be caused by the dominance of adsorption along the grooves of the pair[25] over aggregation in the creation of the adsorbed structure. The force distance curve shows the same oscillations as in the angled cases. This is expected because we observe the same layering of the hydrophobic surfactant beads between the tubes (Figure 3).

The weak layering of the head groups is quite interesting. It is probably caused by the interplay between layering of the tail beads and the connectivity of the beads in the chains. From the local densities, we conclude that all tail beads are involved in the layering. If the tail beads next to the head/tail bond are located in a layer, then the head beads next to the head/tail bond will also be forced into a layer because they are connected via a bond and are repelled by the layered tail beads. The layering is weaker because the effect acts only on the beads next to the head/tail bond and the layers are located far away from the surfaces.

To elucidate the angular dependence of the force, it is necessary to identify its source. To do this, we split the force shown in Figure 2 into its components along the tubes:

$$F(y_i) = \langle \sum_{i=1}^{N} \sum_{k=1}^{N_{beads}} f_z(i, k) \rangle;$$

$$y - \Delta/2 < y(i, k) \leq y + \Delta/2$$

dx.doi.org/10.1021/jp309074c | J. Phys. Chem. B XXXX, XXX, XXX−XXX

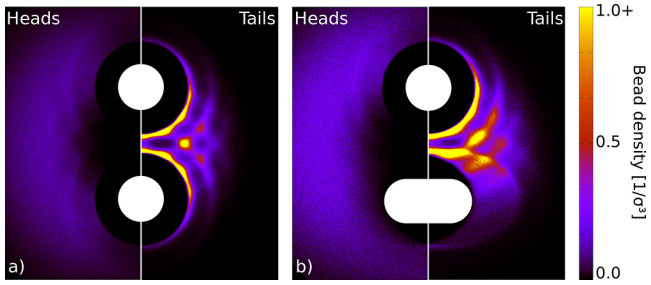

Figure 3. Local density of head beads (left side) and tail beads (right side) in the $x-z$ plane (projection along the y axis): (a) for the parallel case at $d = 4.875\ \sigma$ and (b) for an angle of 45° at the same d. The local densities are calculated in a 2σ thick slab perpendicular to the upper tube and centered at the center of the crossing. Both half-images are symmetric with respect to the z axis (white line). Layering of the hydrophobic tail groups is clearly visible, as indicated by the density oscillations (color code) when moving away from the surface. For the hydrophilic head groups, very weak layering can also be observed (see text).

where y_i is the position along the tube from the center of the crossing and Δ is the length of the interval over which the force is averaged.

In Figure 4, the result of this operation is shown for three selected angles together with the average number of adsorbed hydrophobic beads along the tube. The pronounced dips in the density in Figure 4a for the two angled cases mark the extension of the central aggregate. Because the central aggregate is pinned to the nanotube junction, other adsorbed micelles, which can move freely on the tubes, frequently collide with the central aggregate. The repulsion between the outward-facing hydrophilic head groups then causes a repulsion between these aggregates, leading to the density depletion around the central aggregate. Comparing the extension of the central aggregate with the force along the tube in Figure 4b shows that only the central aggregate contributes to the force. Because there are no structural features that could pin aggregates in the special case of parallel tubes, multiple free-moving "central" aggregates exist, leading to a uniform bead density and accordingly a uniform force distribution.

This explains the result that in the perpendicular case the surfactant-mediated force appears to be concentration-independent above a certain threshold concentration, where the central aggregate forms. In Figure 5a, force curves for two bulk surfactant concentrations 0.3*CMC and 0.5*CMC are shown. The two results are nearly identical. The reason is that for all concentrations larger than 0.2*CMC the central aggregate is fully developed and not affected by the concentration, whereas the adsorbed amount might change dramatically through adsorption along the tubes.[22] Because this region of the tubes does not contribute to the surfactant-mediated tube/tube force, the force remains constant after the creation of the central aggregate. Here we find 255 of 300 and 413 of 500 adsorbed molecules for 0.3*CMC and 0.5*CMC, respectively, whereas the number of surfactant molecules in the central aggregate is ~40 in both cases. For all angled cases, this concentration independence is reproduced, as Figure 5b shows for an angle of 22.5°. The force curves for both concentrations are again very similar, and the average size of the central aggregate is in both cases around 100 molecules. Thus, we have a good reason to assume that the small variations in the bulk

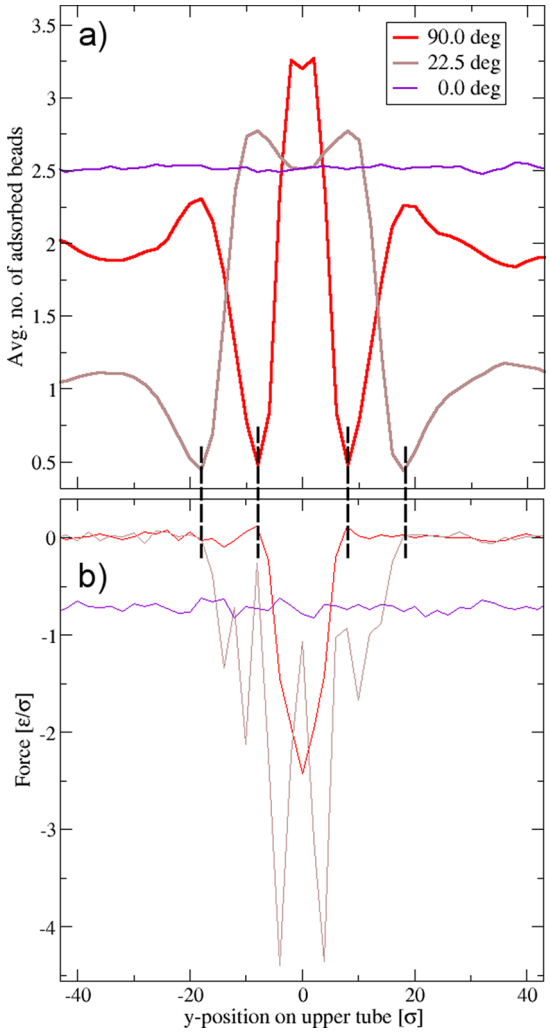

Figure 4. (a) Average number of adsorbed hydrophobic beads per 2 σ long segments of the upper nanotube at a separation distance of 5.125 σ for three different angles as indicated in the Figure. (b) Corresponding local force acting on the upper nanotube for the same angles as in panel a. The pronounced dips in the number of beads mark the boundaries of the central aggregate (dashed vertical lines). Comparison with the force distribution in panel b reveals that the central aggregate is the sole origin of the force.

concentration, which we have to expect between different simulations, do not affect any of our findings.

However, we find that the central aggregate is strongly affected by the geometry of the crossing. The angle dependence of the cluster size distributions of the central aggregate, shown in Figure 6, is a clear indication of this. For the parallel case, the size of the "central aggregate" is determined by the length of the tubes and is therefore ambiguous. Consequently, it cannot be included in Figure 6. The central aggregate is well-defined for all angled cases as the bell-shaped curves indicate. As the angle decreases, the central aggregate grows in size, resulting in a shift of the curves to higher aggregation numbers. This nonlinear size increase with decreasing angle is clearly demonstrated in Figure 6b, where the average size of the central aggregate is plotted versus the tube/tube angle. The nonlinearity of the dependence might not be a surprise because it should be the geometrical size of the covered region that determines the size of the central aggregate rather than the

dx.doi.org/10.1021/jp309074c | J. Phys. Chem. B XXXX, XXX, XXX−XXX

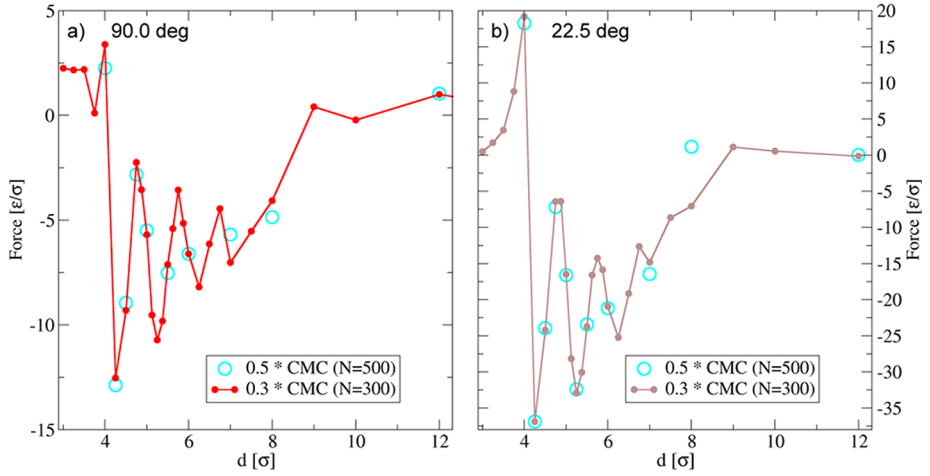

Figure 5. Force−distance curves for two different surfactant bulk concentrations for an angle of (a) 90 and (b) 22.5°, as indicated in the figure, to demonstrate the independence of the force from the concentration.

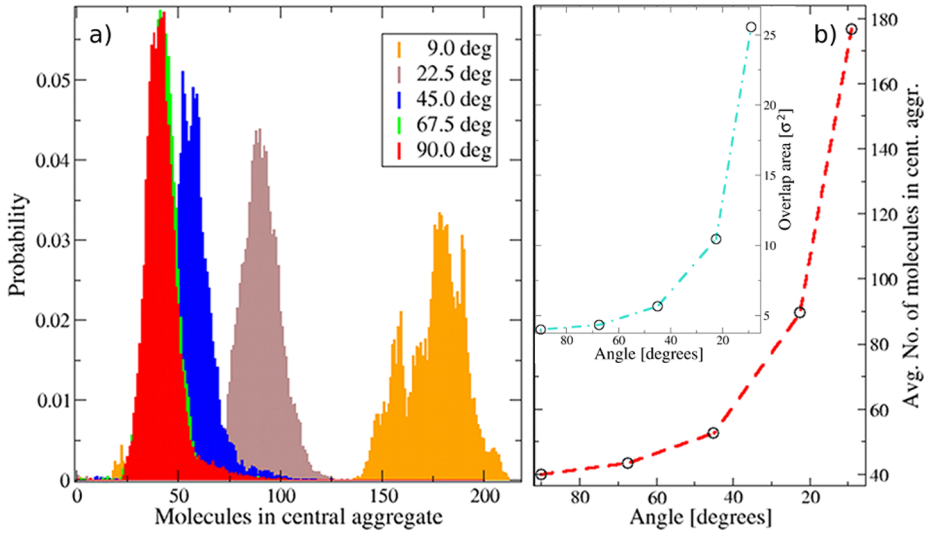

Figure 6. (a) Cluster size distribution of the central aggregate for the five angled cases (9−90°) at a tube/tube separation distance of d = 5.5 σ showing a clear shift to larger aggregates with decreasing tube/tube angle and (b) dependence of the average number of molecules in the central aggregate on the tube/tube angle as well as the overlap area as a function of the angle (inset in panel b) showing the same dependence.

angle between the tubes. However, it is not entirely clear what this "size" should be.

The fact that the central aggregate is responsible for the attraction between the tubes, in combination with its dependence on the size of the crossing, suggests that the forces might also depend on the size of the crossing. A relatively simple connection between the size of the crossing and the strength of the oscillations of the force can be established. Because the force oscillations result from layering of the hydrophobic beads confined between the surfaces, the force should scale linearly with the area over which this layering occurs. In the present case, this area is difficult to determine due to the high curvature of the tubes. As an estimate, we calculate the overlap area that is created when the surfaces of the crossing nanotubes are projected onto the *x*-*y* plane (Figure 1 to the right). For the perpendicular case, this area is a square of area $(2r)^2 = 4\ \sigma^2$. For all others, a rhombus of area $A(\alpha) = (2r)^2/\sin(\alpha)$ is produced. As $\alpha \rightarrow 0°$, the area diverges, as expected for parallel tubes.

To test the hypothesis of the area-dependent force, we plot the surfactant-mediated force for three selected separation distances in the attractive region as a function of the normalized overlap area of the crossing in Figure 8a. The area is normalized with respect to the perpendicular case, that is, by division by $(2r)^2$, leading to a dependence of the normalized area on the angle of $\sin(\alpha)^{-1}$. For all three selected distances, the force depends linearly on the area. This clearly reveals an important structure/function relationship: a larger overlap area leads to a larger central aggregate, which in turn produces stronger forces between the tubes.

The proportionality between the force and the area at a given tube/tube separation d suggests that there is a stress:

$$\sigma_z(d) = \frac{f(d, \alpha)}{A(\alpha)} = \frac{f(d, \alpha)}{4r^2/\sin(\alpha)}$$

that depends only on the tube/tube separation d such that

$$f(d, A) = A(\alpha)*\sigma_z(d)$$

Because the slopes in Figure 8a depend on the tube/tube separation d, $\sigma_z(d)$ indeed depends on d. This suggests that the complex force data $f(d,\alpha)$ can be collapsed onto a stress master

dx.doi.org/10.1021/jp309074c | J. Phys. Chem. B XXXX, XXX, XXX−XXX

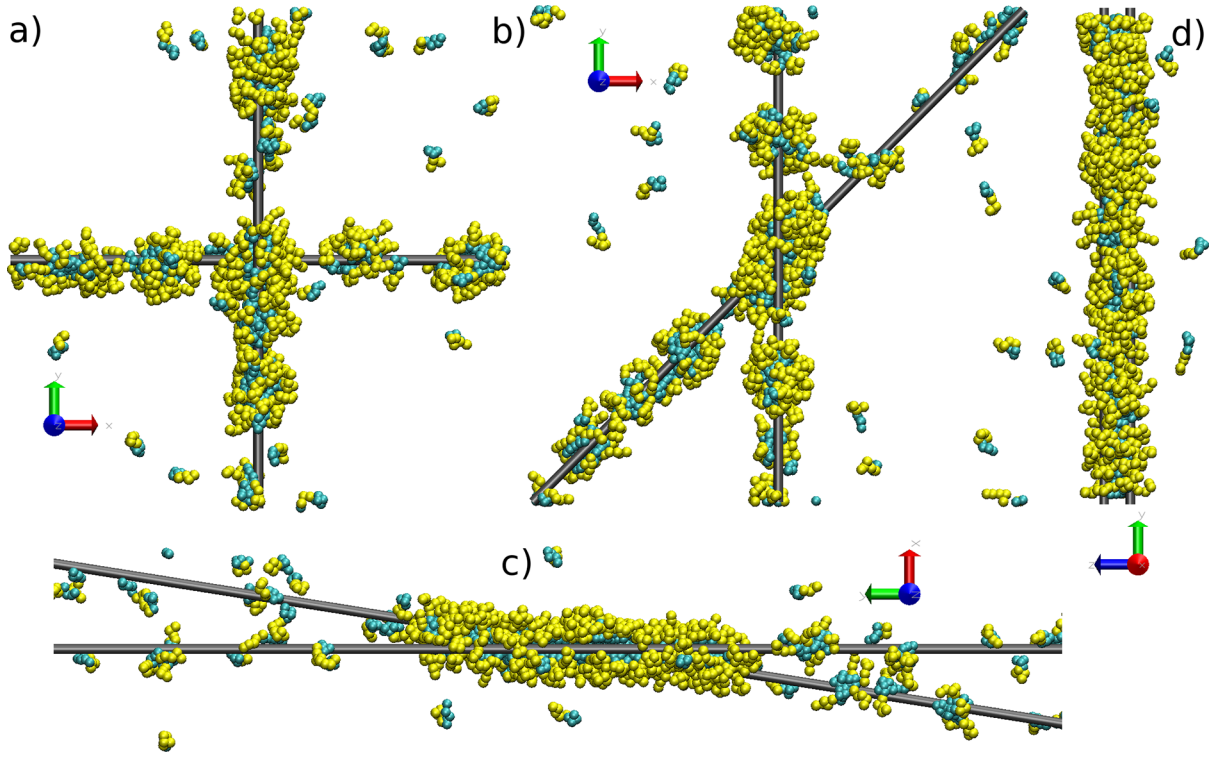

Figure 7. Snapshots showing the system at a tube/tube separation distance of 5.5 σ for the perpendicular case (90°) (a), 45° (b), 9° (c), and the parallel case (0°) (d). The dependence of the size and shape of the central aggregate on the nanotube angle is clearly recognizable. The snapshots were produced using the VMD software package.[28]

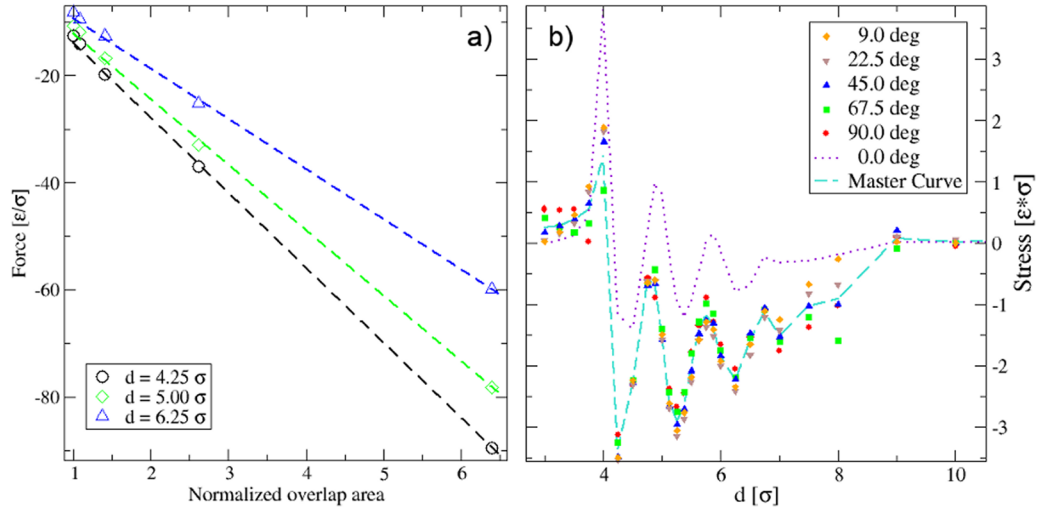

Figure 8. Scaling behavior of the force: (a) Surfactant-mediated force for three selected tube/tube separation distances over the normalized overlap area of the junction; a nearly linear behavior is observed for all three distances. The area is given in terms of 4 σ^2, the overlap area in the perpendicular case. (b) Stress versus distance curves obtained by dividing the force curves in Figure 2a by the overlap area for all angles. A master curve is obtained by averaging of the stresses at fixed d over all angles (9−90°). At fixed d, most data points coincide with the average, thus proving that the scaling law is valid.

curve $\sigma_z(d)$. This master curve is shown in Figure 8b together with all simulation data. It is obtained by averaging over the stresses of all angled cases at a given tube/tube separation. The result clearly suggests that such a master curve exists. This in turn proves that the surfactant-mediated force scales linearly with the area between the tubes.

Intriguingly, the parallel case does not follow that pattern. However, the stress curve for the parallel case can be shifted such that the oscillations overlap with those of the master curve. This is consistent with our expectations and understanding of the structure/function relationship of layering. At the same time, it re-emphasizes that in the parallel case the overall attraction is absent. It should be noted that the master curve in Figure 8 is specific to the surfactant H5T5. However, other surfactants (e.g., H10T5) can produce a similar master curve as long as they form similar structures, that is, a central aggregate on the nanotube junction.

dx.doi.org/10.1021/jp309074c | J. Phys. Chem. B XXXX, XXX, XXX−XXX

CONCLUSIONS

We have studied the dependence of surfactant-mediated forces between carbon nanotubes on the angle and the distance between the tubes using DPD simulations.

For all angles larger than zero, we find an overall attractive force between the tubes exerted by the central aggregate at the nanotubes' junction for a large distance interval $4\ \sigma < d < 9\ \sigma$. This is in accordance with the results of ref 25, where for a perpendicular arrangement of the tubes the attraction was shown to originate from restoring forces opposing the stretching of the central aggregate. Strong oscillations of the force caused by layering were found at all angles.

The amplitude of these oscillations and the magnitude of the overall attraction showed a strong dependence on the angle; however, we rationalize that the surfactant-mediated force should rather depend on the central aggregate's size, which in turn depends on the size of the tube/tube crossing. Using the overlap area between the tubes as a measure for the size of the central aggregate, we normalize all forces with this overlap area and observe that they collapse onto a stress master curve $\sigma_z(d)$. This is important because it allows us to calculate the surfactant-mediated force between the tubes for an arbitrary angle and distance from the master curve $\sigma_z(d)$ and the explicit angle dependence

$$f(d, \alpha) = \sigma_z(d)A(\alpha) = \sigma_z(d)4r^2/\sin(\alpha)$$

However, for the parallel case, the simulations showed a different behavior, that is, an almost complete lack of the overall attractive region. Because aggregation and adsorption seem to be different for this case, leading to a concentration dependence of the force, for example, it is necessary to treat the parallel case separately.

Beyond their contribution to broaden our understanding of directed self-assembly, the findings presented in this article are a key prerequisite to calculate the behavior of surfactant reinforced carbon nanotube networks. This is important to gain essential insights for the realization of such materials and their applicability in industry.

AUTHOR INFORMATION

Corresponding Author

*Tel: +44 (0)131 451 3074. E-mail: dm313@hw.ac.uk.

Notes

The authors declare no competing financial interest.

ACKNOWLEDGMENTS

D.M. is grateful for financial support for this project through the German Science Foundation's (DFG) research stipend MU 3236/1 "Multiscale modeling of surfactant reinforced carbon nanotube networks".

REFERENCES

(1) Salvetat, J. D.; Rubio, A. *Carbon* **2002**, *40*, 1729−34.
(2) Cveticanin, J.; Joksic, G.; Leskovac, A.; Petrovic, S.; Sobot, A. V.; Neskovic, O. *Nanotechnology* **2010**, *21*, 015102.
(3) Mahmood, M.; et al. *Nanomedicine* **2009**, *4*, 883−893.
(4) Liu, Z.; Tabakman, S.; Welsher, K.; Dai, H. *Nano Res.* **2009**, *2*, 85−120.
(5) Capek, I. *Adv. Colloid Interface Sci.* **2009**, *150*, 63−89.
(6) Cheung, W.; Chiu, P. L.; Parajuli, R. R.; Ma, Y.; Ali, S. R.; He, H. *J. Mater. Chem.* **2009**, *19*, 6465−6480.
(7) Blighe, F. M.; Young, K.; Vilatela, J. J.; Windle, A. H.; Kinloch, I. A.; Deng, L.; Young, R. J.; Coleman, J. N. *Adv. Funct. Mater.* **2011**, *21*, 364−371.
(8) Young, K.; Blighe, F. M.; Vilatela, J. J.; Windle, A. H.; Kinloch, I. A.; Deng, L.; Young, R. J.; Coleman, J. N. *ACS Nano* **2010**, *4*, 6989−6997.
(9) Wang, X.; Li, Q.; Xie, J.; Jin, Z.; Wang, J.; Li, Y.; Jiang, K.; Fan, S. *Nano Lett.* **2009**, *9*, 3137−3141.
(10) Giordani, S.; Bergin, S.; Nicolosi, V.; Lebedkin, S.; Blau, W. J.; Coleman, J. N. *Phys. Stat. Sol. B* **2006**, *243*, 3058−3062.
(11) Wang, H.; Zhou, W.; Ho, D. L.; Winey, K. I.; Fischer, J. E.; Glinka, C. J.; Hobbie, E. K. *Nano Lett.* **2004**, *4*, 1789−1793.
(12) Yurekli, K.; Mitchell, C. A.; Krishnamoorti, R. *J. Am. Chem. Soc.* **2004**, *126*, 9902−9903.
(13) Matarredona, O.; Rhoads, H.; Li, Z.; Harwell, J.; Balzano, L.; Resasco, D. *J. Phys. Chem. B* **2003**, *107*, 13357−13367.
(14) Utsumi, D.; Kanamaru, M.; Honda, H.; Kanoh, H.; Tanaka, H.; Ohkubo, T.; Sakai, H.; Abe, M.; Kaneko, K. *J. Colloid Interface Sci.* **2007**, *328*, 276−284.
(15) Shvartzman-Cohen, R.; Florent, M.; Goldfarb, D.; Szleifer, I.; Yerushalmi-Rosen, R. *Langmuir* **2008**, *24*, 4625−4632.
(16) Lin, S.; Blankschtein, D. *J. Phys. Chem. B* **2010**, *114*, 15616−15625.
(17) Tummala, N. R.; Morrow, B. H.; Resasco, D. E.; Striolo, A. *ACS Nano* **2010**, *4*, 7193−7204.
(18) Xu, Z.; Yang, X.; Yang, Z. *Nano Lett.* **2010**, *10*, 985−991.
(19) Angelikopoulos, P.; Bock, H. *J. Phys. Chem. Lett.* **2011**, *2*, 139−144.
(20) Angelikopoulos, P.; Bock, H. *Phys. Chem. Chem. Phys.* **2012**, *14*, 9546−9557.
(21) Angelikopoulos, P.; Gromoy, A.; Leen, A.; Nerushev, O.; Bock, H; Campbell, E. E. B. *J. Phys. Chem. C* **2010**, *114*, 2−9.
(22) Angelikopoulos, P.; Bock, H. *J. Phys. Chem. B* **2008**, *112*, 13793−13801.
(23) Angelikopoulos, P.; Al Harthy, S.; Bock, H. *J. Phys. Chem. B* **2009**, *113*, 13817−13824.
(24) Angelikopoulos, P.; Schou, K.; Bock, H. *Langmuir* **2010**, *26*, 18874−18883.
(25) Angelikopoulos, P.; Bock, H. *Langmuir* **2010**, *26*, 899−907.
(26) Groot, R. D.; Warren, P. B. *J. Chem. Phys.* **1997**, *107*, 4423−4435.
(27) Jordanovic, J.; Klapp, S. H. L. *Phys. Rev. Lett.* **2008**, *101*, 038302.
(28) Humphrey, W.; Dalke, A.; Schalke, K. *J. Molec. Graphics* **1996**, *14.1*, 33−38.